NJC

ROYAL SOCIETY OF CHEMISTRY

PAPER

View Article Online
View Journal | View Issue

Cite this: *New J. Chem.*, 2021, **45**, 3271

A novel pH-responsive Fe-MOF system for enhanced cancer treatment mediated by the Fenton reaction†

Senlin Wang,‡[a] Hongshuai Wu,‡[a] Kai Sun,[a] Jinzhong Hu,[a] Fanghui Chen,[a] Wen Liu,[a] Jian Chen,[a] Baiwang Sun *[a] and Abul Monsur Showkot Hossain*[b]

Received 17th October 2020,
Accepted 7th January 2021

DOI: 10.1039/d0nj05105e

rsc.li/njc

Recently, the toxic hydroxyl radical (·OH) has received wide interest for inducing cell apoptosis by increasing the intracellular reactive oxygen species (ROS) levels. Herein, a cationic polymer (MV-PAH) was rationally synthesized, and a new pH-responsive nanoreactor (DOX@Fe-MOF@PEM) was modified with the prepared cationic polymer MV-PAH multilayers by layer-by-layer (LBL) technique. The polyelectrolyte multilayer (PEM) disassembled and notably enhanced drug delivery in the weak acid environment of the tumor cell. In the cytotoxicity and apoptosis experiments, DOX@Fe-MOF@PEM revealed an advanced repression of cancer. The H_2O_2 induced by DOX and MV-PAH could be catalyzed to generate hypertoxic ·OH through intracellular iron ions based on a Fenton-like reaction, which thereby improved the anticancer effect of DOX. This realistic strategy may create a potential way to provide a combination of ROS and chemotherapy to improve the anti-cancer effect.

1. Introduction

Oxidation and antioxidants in healthy humans are in dynamic equilibrium, and the body usually maintains suitable levels of ROS.[1,2] Breaking the threshold of ROS levels causes oxidative damage to cells, leading to apoptosis or necrosis.[3–6] According to recent reviews, ROS play a critical role in the therapeutic effects and side effects of chemotherapy agents.[7–10] Many studies have shown that chemotherapy drugs, such as doxorubicin (DOX) and cisplatin, can mediate the activation of nicotinamide adenine dinucleotide phosphate (NADPH) oxidase (NOX), thereby triggering the conversion of oxygen to superoxide radicals ($O_2^{\bullet -}$), which further generate H_2O_2 through the superoxide dismutase enzyme.[11,12] Through the Fenton reaction mediated by Fe^{2+}/Fe^{3+}, H_2O_2 could be catalyzed to produce highly reactive ·OH, which may cause oxidative damage to cancer cells' lipids, proteins and DNA, thereby improving the anticancer activity of chemotherapy drugs.[11–14] This route also guides the way for the development of chemotherapy drugs in the future.[13,15–18]

Chemotherapy drugs play a vital role in the treatment of malignant tumors, but their serious side effects (nausea, ototoxicity and nephrotoxicity) have limited further clinical application.[19–21] The great advances in nanoscience have established the tremendous latent clinical capacity of nanomaterials.[22] Targeted administration can selectively transport cytotoxic drug molecules to the target site, which is an effective method for reducing systemic toxic side effects and improving the therapeutic effects.[23,24] A switchable "gatekeeper" that intelligently controls drug release *via* specific stimuli can appreciably heighten the therapeutic effect of drugs.[25]

The polyelectrolyte pair, usually consisting of the polycation polyallylamine hydrochloride (PAH) and polystyrene sulfonate (PSS), forms a type of polyelectrolyte multilayer (PEM), which is gradually fabricated as a multilayered ultrathin film by layer-by-layer (LBL) technology.[26,27] Due to its effectivity, biocompatibility and accessibility, the PEM has already received widespread attention in the fields of biomaterials.[22,28] Our group earlier developed a hollow mesoporous silica nanoparticle (HMSN@PEM) with a pH-sensitive PEM coating to realize the specific release of DOX and glucose oxidase in the tumor microenvironment for combined starvation and also drug therapy.[29,30]

Methyl viologen (MV or PQ) is a bipyridyl herbicide. Intriguingly, the genotoxicity and cytotoxicity of MV may be related to its ability to generate ROS. It has already been firmly established as an electron acceptor that acts on the redox reaction in cells to generate a large number of active free radicals, causing lipid peroxidation of cell membranes and oxidative damage of tissue cells.[31,32] Drawing on this idea, herein, we first confirmed the synthesis of a cationic

[a] *School of Chemistry and Chemical Engineering, Southeast University, Nanjing 211189, P. R. China. E-mail: chmsunbw@seu.edu.cn*
[b] *School of Chemistry and Chemical Engineering, Jiangsu University, Zhenjiang, Jiangsu 212013, P. R. China. E-mail: monsur_12@yahoo.com*

† Electronic supplementary information (ESI) available. See DOI: 10.1039/d0nj05105e

‡ These authors have contributed equally to the work.

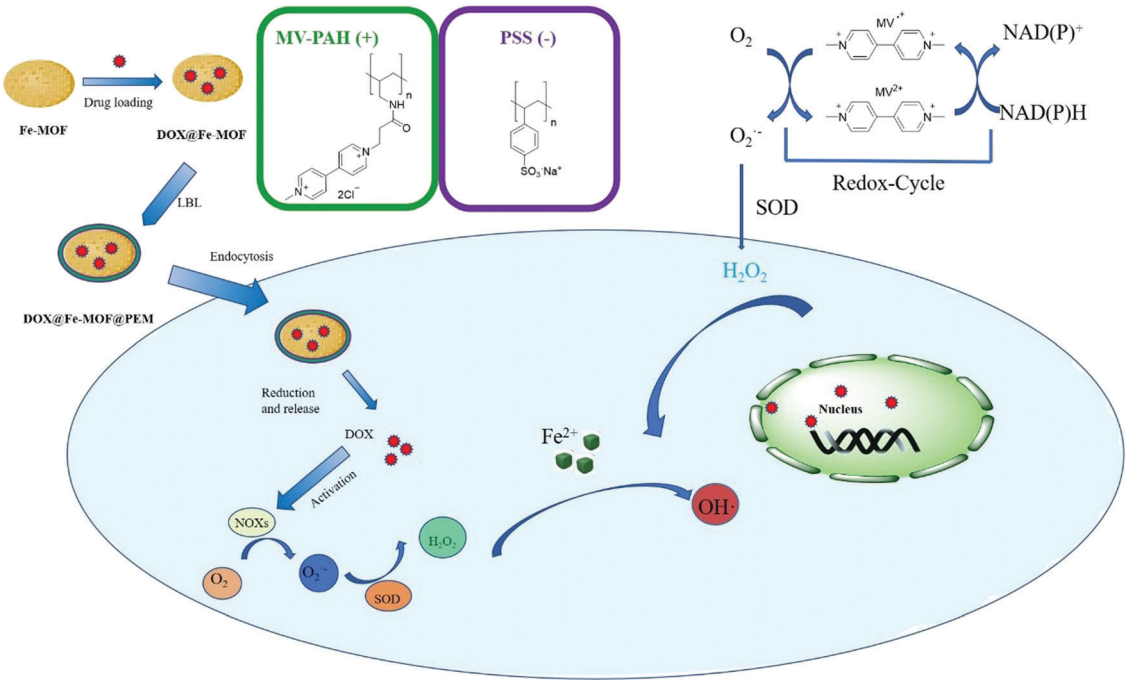

Scheme 1 A novel pH-responsive Fe-MOF system for enhancing cancer treatment mediated by a Fenton reaction.

polymer (MV-PAH), then constructed a novel pH-responsive Fe-MOF system modified with MV-PAH by LBL technique, encapsulating the chemotherapeutic DOX for enhanced cancer treatment mediated by a Fenton reaction. As shown in Scheme 1, DOX and iron were released by the iron-based MOF nanoparticle in the weak acid environment of the tumor cell. Then, H_2O_2 induced by DOX and MV could be catalyzed to generate •OH by intracellular iron ions, resulting in enhanced antitumor activity. Such a smart drug-delivery nanosystem may provide a promising candidate for elevated cancer therapy.

2. Experimental section

2.1. Materials

3-(4,5-Dimethyl-thiazol-2-yl)-2,5-diphenyltetrazolium bromide (MTT), poly(sodium 4-styrenesulfonate) (PSS, M_w = 70 000), doxorubicin hydrochloride (DOX), 2′,7′-dichlorofluorescin diacetate (DCFH-DA), 2-aminoterephthalic acid, poly(allylamine hydrochloride) (PAH, M_w = 15 000), 4,4′-bipyridine and 3-bromopropionic acid were supplied by Sigma-Aldrich Chemical Company (St. Louis, MO). V-FITC/PI was obtained from Beyotime Biotechnology (Haimen, Jiangsu, China). The rest of the materials were commercially available.

2.2. Synthesis of MV-PAH

MV-PAH was prepared by a three-step process as illustrated in Scheme 2.

First, 1-methyl-4,4′-bipyridinium iodide (**1**) was prepared according to the procedure found in literature.[33,34] To a solution of 4,4′-dipyridyl (1.56 g, 10 mmol) in acetonitrile (30 mL) was added methyl iodide (1.42 g, 10 mmol), and the reaction mixture was stirred at room temperature for 12 h. The product was collected by filtration and washed with acetonitrile to obtain a pure yield of orange powder. Yield: 85.9% (2.56 g, 8.59 mmol). M.p. = 247–248 °C; ^{1}H NMR (600 MHz, DMSO) δ 9.18 (d, J = 6.5 Hz, 2H), 8.88 (dd, J = 4.6, 1.5 Hz, 2H), 8.65 (d, J = 6.7 Hz, 2H), 8.07 (dd, J = 4.5, 1.6 Hz, 2H), 4.42 (s, 3H).

In the second step, 1-(2-carboxyethyl)-1′-methyl-4,4′-bipyridinium dichloride (**2**) was synthesized according to the literature with some modifications.[35,36] Briefly, to a solution of complex **1** (1.49 g, 5 mmol) in acetonitrile (30 mL) was added 3-bromopropionic acid (3.06 g, 20 mmol), and the reaction mixture was heated to reflux and stirred for 24 h. The reaction mixture was filtered and also washed with acetonitrile. The residue was dissolved in THF (5 mL) and precipitated from hexane (20 mL), and then dissolved in water, then NH_4PF_6 solution was added to replace the counter-anion with PF_6^-. The PF_6^- salt was filtered, washed with water, and dried under vacuum overnight. The PF_6^- salt was then dissolved in CH_3CN, and tetraethylammonium chloride was added to replace the counter-anion with Cl^- to yield a red powder, which was dried *in vacuo*. Yield: 50% (0.32 g, 0.60 mmol). ^{1}H NMR (600 MHz, D_2O) δ 9.07 (d, J = 6.9 Hz, 2H), 8.95 (d, J = 6.8 Hz, 2H), 8.44 (d, J = 6.8 Hz, 2H), 8.43 (d, J = 6.8 Hz, 2H), 4.87 (t, J = 6.4 Hz, 2H), 4.40 (s, 3H), 3.04 (t, J = 6.4 Hz, 2H).

For the synthesis of MV-PAH, complex **2** (200 mg, 0.61 mmol), EDC (128.2 mg, 0.67 mmol) and NHS (76.9 mg, 0.67 mmol) were dissolved in 5 mL of water. Then, PAH (84 mg, 5.6 μmol) was injected, and the purification was carried out by dialysis (MWCO = 3000 Da) after the mixture was stirred overnight. The product was lyophilized and analyzed using spectroscopic techniques.

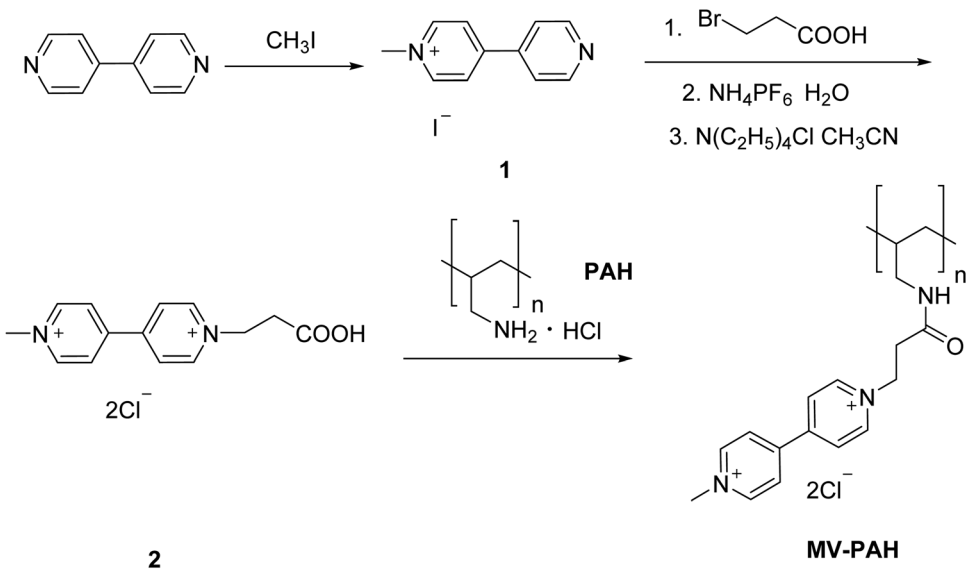

Scheme 2 Synthesis route of MV-PAH.

2.3. Preparation of Fe-MOF nanoparticles

Fe-MOF nanoparticles were prepared according to the procedure in the literature, with slight modifications.[15] First, to a solution of Pluronic F-127 (320 mg) and $FeCl_3 \cdot 6H_2O$ (357 mg, 1.32 mmol) in Milli-Q water (30 mL) was added acetic acid (0.8 mL). Later, 2-aminoterephthalic acid (120 mg, 0.66 mmol) was injected after the mixture was stirred for an hour. Finally, the mixture was transferred to an autoclave and heated for 20 h at 110 °C and then the mixture was stirred for a further 1 h. The nanoparticles were collected and washed several times using Milli-Q water and ethanol by centrifuging at 8000 rpm for 15 minutes, yielding Fe-MOF nanoparticles as brown powders after drying under vacuum.

2.4. Preparation of DOX@Fe-MOF@PEM nanoparticles

As shown in Scheme 1, DOX@Fe-MOF@PEM (DOX@Fe-MOF@PSS@MV-PAH@PSS) nanoparticles were formulated according to a previous work with slight modifications.[11]

For DOX loading, DOX (10 mg) and Fe-MOF (20 mg) were dispersed in PBS (20 mL), then stirred overnight at room temperature in the dark. Then, DOX@Fe-MOF was collected and washed with PBS by centrifugation (7000 rpm, 10 min). Note that DOX concentrations in the supernatant liquid samples were measured by UV-Vis spectroscopy using a DOX standard curve.

For polyelectrolyte multilayer coating on the surfaces of DOX@Fe-MOF, DOX@Fe-MOF@PEM was prepared by the LBL technique according to our past work.[29] Briefly, PSS and MV-PAH were dissolved in 0.5 M NaCl (2 mg mL^{-1}). DOX@Fe-MOF solution (2.0 wt%, 20 mL) was added to the negatively charged PSS solution (20 mL), and the mixture was stirred for 2 h. The particles were collected by centrifugation (6000 rpm, 8 min), cleaned and dispersed in table salt. Then, 20 ml of positively charged MV–PAH was injected and stirred for another 2 h, centrifuged, cleaned and suspended with the table salt (2 mg mL^{-1} NaCl), and another PSS layer was repeated and alternately coated on the surface of collection.

To determine the DOX loading, the supernatant and the washing solutions were measured using a Jasco V530 UV-Vis spectrophotometer, with a standard curve method, at the wavelength of 480 nm. The drug loading capacity (DLC) was calculated by the following formula:

$$\mathrm{DLC}\ (\%) = \frac{\text{Weight of drug in nanoparticles}}{\text{Weight of total nanoparticles}} \times 100$$

The Brookhaven A8530 instrument was used to determine the size and zeta potential of the nanoparticles by dynamic light scattering (DLS). The surface charge of the nanoparticles was tested by a Zeta Plus zeta potential analyzer. A JEM-100CXII transmission electron microscope was used to observe the surface morphology of the prepared nanoparticles through a transmission electron microscope (TEM) at 25 °C with an acceleration voltage of 180 kV. The pore size distribution and surface area of Fe-MOF were studied using a nitrogen (N_2) adsorption–desorption method, which was carried out on a Brunauer–Emmett–Teller Micromeritics Tristar 3000 analyzer. The iron mass of the particles was investigated using an ICP-MS 7400 instrument.

2.5. Stability of DOX@Fe-MOF@PEM nanoparticles

The prepared DOX@Fe-MOF and DOX@Fe-MOF@PEM nanoparticles were maintained at 4 °C for a particular time. The stability was studied by monitoring changes in nanoparticle size and PDI at particular time intervals (after 3, 7, 14, 21 and 28 days). Furthermore, the nanoparticle suspension was centrifuged at 2000 rpm for 8 minutes to make sure that impurities were settled as planned, and then a 3 mL aliquot extracted from the supernatant was investigated. The PDI and size of nanoparticles were measured by DLS. Each sample was tested in triplicate.

2.6. *In vitro* pH-triggered drug release

The drug release of the prepared DOX@Fe-MOF and DOX@Fe-MOF@PEM was performed using dialysis bag diffusion technology. Briefly, the prepared nanoparticles were suspended in 4 mL PBS (pH = 5.5 and 7.4). The suspension was then placed in a dialysis bag (MWCO = 3000 Da), and the dialysis process was observed against PBS at 25 °C in the dark under constant stirring. The released mass of DOX was determined by comparing the specific absorption peak obtained using UV-vis with the standard curve.

2.7. •OH generation

Measurements were carried out according to a previous report[15] with slight modifications. Briefly, different concentrations of Fe-MOF (0, 5, 10, 20, 40, and 80 μg mL^{-1}) were added to 10 mL PBS buffer solution (pH 5.5) containing H_2O_2 (1 mM) and 3,3′,5,5′-tetramethylbenzidine (TMB, 0.25 mM) and maintained at 37 °C for 5 min. The absorbance spectra were observed using UV-vis spectroscopy.

2.8. Cellular uptake

Confocal laser scanning microscopy (CLSM) was employed to qualitatively measure the cell interaction with the nanoparticles DOX@Fe-MOF and DOX@Fe-MOF@PEM. Briefly, the cells (A549) were placed at a density of approximately 1×10^5 cells per dish in a *Φ*20 mm confocal laser dish. After overnight culture, the cells were incubated with DOX@Fe-MOF and DOX@Fe-MOF@PEM nanoparticles. After 4 h incubation, the medium was poured out, and the cells were washed with PBS three times. Finally, the cells were stained with DAPI and incubated for 15 min. The intracellular distribution of nanoparticles was then cautiously observed with CLSM.

2.9. ROS generation

To determine the formation of ROS, DCFH-DA, a fluorogenic substrate that could be oxidized by ROS to the highly fluorescent dichlorofluorescein (DCF), was selected to detect the intracellular production of ROS. In short, on the day before treatment, A549 cells were grown in a 96-well plate at a density of 2×10^5 cells per well in 200 μL of complete cell culture medium. Cells were also pretreated with various formulations for 24 h. Then, the culture media were replaced with PBS. After that, 200 μL of fresh culture media containing 20 μM DCFH-DA was added to each well for 30 min for dye loading at 37 °C. Eventually, the cells were quantified by flow cytometry after washing twice with fresh medium.

2.10. *In vitro* cytotoxicity

The cells (A549 and MCF-7) were seeded at a density of 6×10^3 cells per well. The cells were exposed to free DOX, Fe-MOF, DOX@Fe-MOF and DOX@Fe-MOF@PEM formulations at different DOX concentrations (2.5, 5, 10, 20, and 40 mg mL^{-1}) for 24 h at 37 °C. Each well was injected with 150 μL MTT solution (5.0 mg ml^{-1}) and also incubated for 4 h at 37 °C. Subsequently, the medium was replaced with 150 μL DMSO to dissolved the resultant purple crystals. Then, the plates were shaken on the table concentrator for 15 min. Finally, the absorption at 490 nm was measured by a microplate reader.

2.11. Cell apoptosis

For apoptosis, A549 cells were cultured at a density of approximately 1×10^5 cells per well for 24 h. Later, the cells were incubated with DOX, DOX@Fe-MOF, and DOX@Fe-MOF@PEM

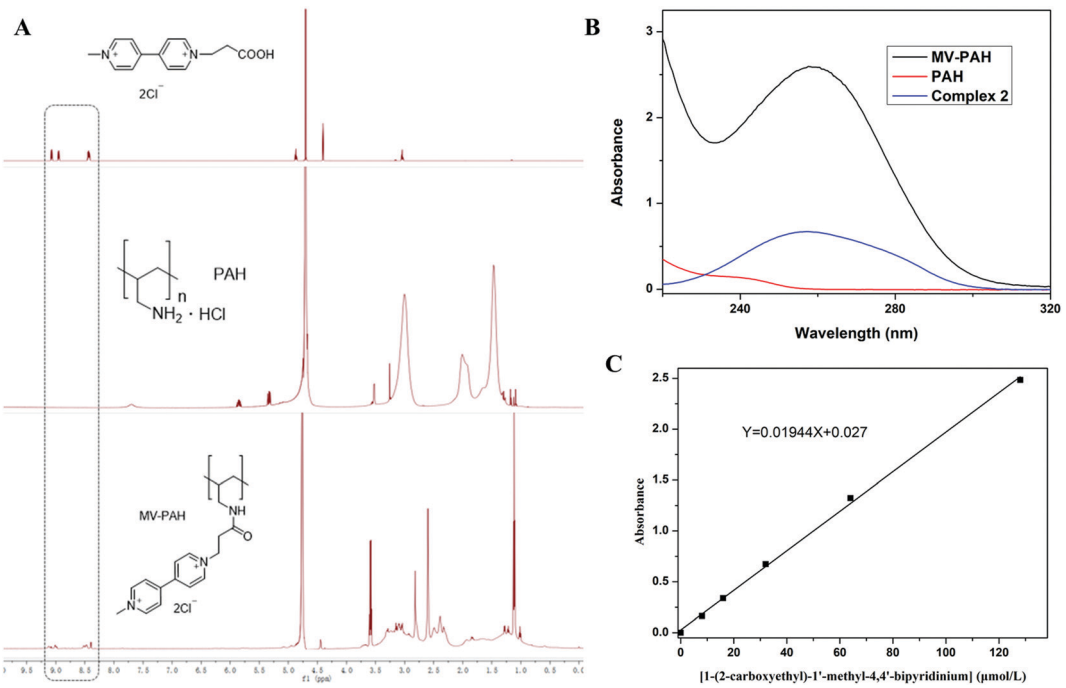

Fig. 1 (A) ^{1}H NMR spectra of complex **2**, PAH and MV-PAH; (B) UV-vis spectroscopy of MV-PAH, PAH and complex **2** in aqueous solution; (C) UV calibration curve of 1-(2-carboxyethyl)-1′-methyl-4,4′-bipyridinium dichloride in water at λ = 257 nm.

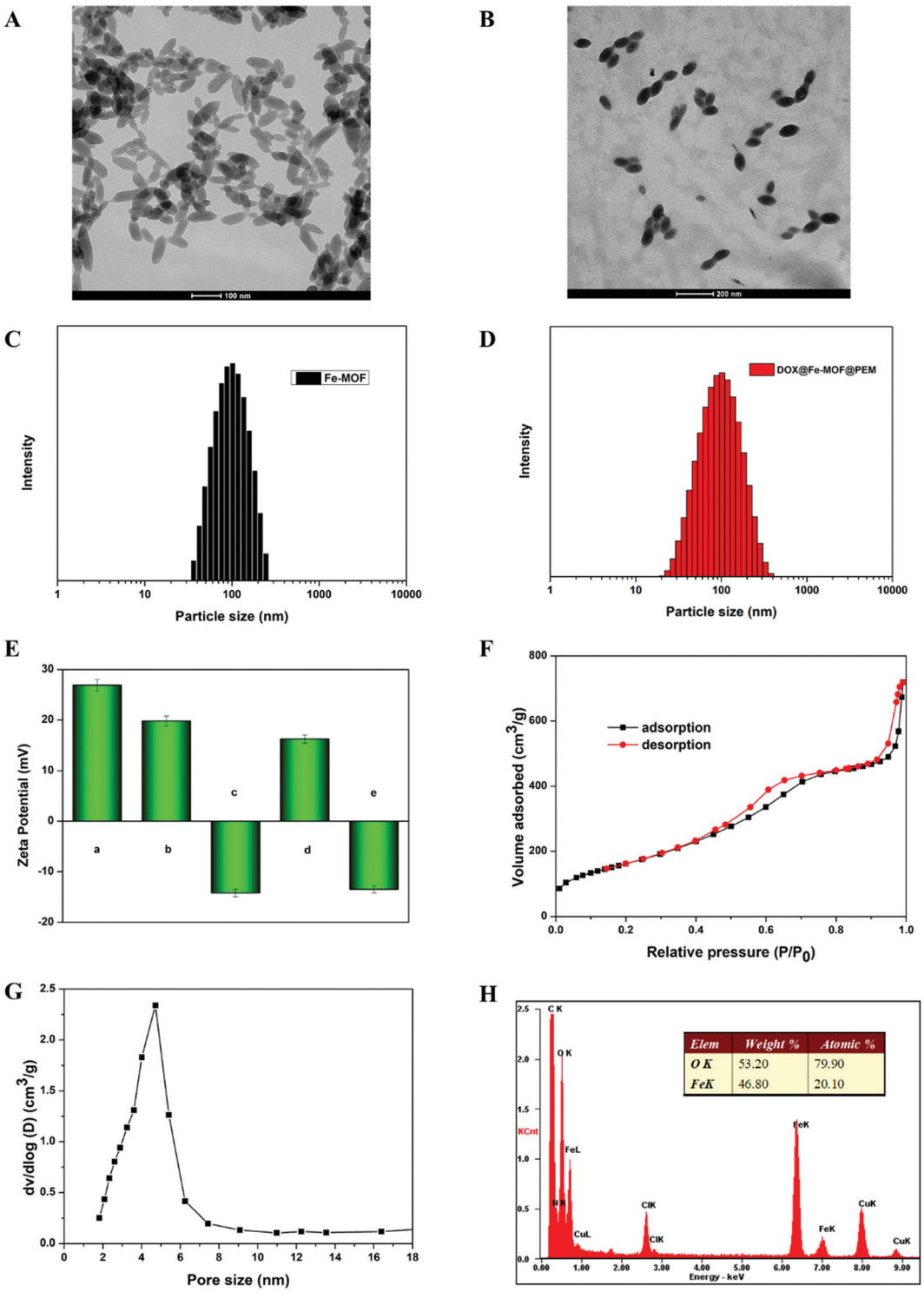

Fig. 2 (A) TEM image of Fe-MOF; (B) TEM image of DOX@Fe-MOF@PEM; (C) size distribution of Fe-MOF; (D) size distribution of DOX@Fe-MOF@PEM; (E) zeta potential of nanoparticles (a: Fe-MOF, b: DOX@Fe-MOF, c: DOX@Fe-MOF@PSS, d: DOX@Fe-MOF@PSS@MV-PAH, e: DOX@Fe-MOF@PEM); (F) N_2 isotherm of pristine Fe-MOF at 77 K; (G) pore size distribution of pristine Fe-MOF derived from N_2 isotherm data and (H) the EDX analysis for Fe and O elements of Fe-MOF.

particles at the same dosage of 2.5 μg mL^{-1} DOX, respectively. After 24 h of incubation, cells were harvested, washed twice, and resuspended with PBS. The Annexin V-FITC apoptosis detection kit was used for apoptosis, quantified by flow cytometry.

3. Results and discussion

3.1. Preparation of MV-PAH

The preparation of MV-PAH is represented in Scheme 2. First, 1-methyl-4,4′-bipyridinium iodide (**1**) was prepared by alkylation

reaction, and the typical ^{1}H NMR spectra is depicted in Fig. 1A. As expected, all characteristic peaks could be observed, in good agreement with the previous report. Next, complex (**1**) was reacted with 3-bromopropionic acid counter-anion, and subsequent ion exchange gave MV-COOH (**2**). Finally, complex (**2**) was conjugated to PAH through a condensation reaction of carboxyl and amino groups. As depicted in Fig. 1A, MV-PAH exhibited the same chemical shifts at δ 8.43–9.07 ppm as complex **2**, which was attributed to aromatic hydrogen protons, indicating the successful conjugation of MV-COOH to PAH. Furthermore, as visible in Fig. 1B, the UV absorption of the MV-grafted polymer had a baseline shift at 257 nm, which could be ascribed to the characteristic UV absorbance peak of 1-(2-carboxyethyl)-1'-methyl-4,4'-bipyridinium dichloride at this wavelength, suggesting that the successful combination of MV-COOH and PAH was confirmed. To determine how much methyl viologen was grafted onto the polymer, a calibration curve of 1-(2-carboxyethyl)-1′-methyl-4,4′-bipyridinium dichloride in water was created in Fig. 1C. Using this technique, it could be determined that on average, six methyl viologen entities were grafted to one polymer chain.

3.2. Synthesis and characterization of Fe-MOF nanoparticles and DOX@Fe-MOF@PEM nanoparticles

In this work, the DOX@Fe-MOF@PEM nanoparticles were fabricated *via* a three-step procedure. Initially, Fe-MOF nanoparticles were formulated according to previous literature with slight modifications. Then, the prepared Fe-MOF nanoparticles were packaged with DOX for anticancer drug loading. Finally, the formed DOX-loaded Fe-MOF was coated with polyelectrolyte multilayers (PSS and MV-PAH) by the layer-by-layer technique. TEM images of Fe-MOF and DOX@Fe-MOF@PEM nanoparticles are displayed in Fig. 2A and B. The Fe-MOF nanoparticles were produced from an aqueous reaction mixture of $FeCl_3{\cdot}6\ H_2O$ and H_2N–BDC, with needle-shaped morphology of an average length of 95 nm and width of 42 nm. Compared with Fe-MOF, the size of DOX@Fe-MOF@PEM was almost same as the unmodified example, but the surfaces have coated polyelectrolyte multilayers of ~3 nm. Moreover, dynamic light scattering measurements for the hydrodynamic sizes of Fe-MOF and DOX@Fe-MOF@PEM were 102 nm and 110 nm (Fig. 2C and D), respectively. The average size determined by DLS of DOX@Fe-MOF@PEM was larger than that of Fe-MOF, which was attributed to hydration layers around the particle surface in aqueous solution. Further experiments were performed to measure the zeta potential of the resulting nanoparticles. The polyelectrolyte multilayers (PSS and MV-PAH) coating the nanoparticles remarkably changed the zeta potential; the values were 26.9, 19.8, −14.2, 16.3 and −13.5 mV for Fe-MOF, DOX@Fe-MOF, DOX@Fe-MOF@PSS, DOX@Fe-MOF@PSS@MV-PAH and DOX@Fe-MOF@PEM, respectively (Fig. 2E). N_2 adsorption–desorption measurements are depicted in Fig. 2F and G; the surface area and pore size were calculated to be 592.2 $m^2\ g^{-1}$ and 5.4 nm, respectively. The EDX analyses of Fe and O element of Fe-MOF are shown in Fig. 2H. According to the UV-Vis standard curve method at the wavelength of 480 nm, the DLC of DOX in DOX@Fe-MOF@PEM was calculated to be a decent rate (88.4%), which could be attributed to its large cavity and specific surface area.

3.3. Stability and *in vitro* drug release

The physical stability of DOX@Fe-MOF@PEM was also determined. After 4 weeks of storage in PBS, the DOX@Fe-MOF@PEM solution remained clear, without any significant precipitation. In addition, as shown in Fig. 3A, the sizes remained stable, and the PDI also remained at a favorable level, which may be due to the stereospecific block of the PEM. The results reveal the favorable physical stability of nanoparticles under normal physiological conditions, indicating they might be used for a long duration of circulation time in the bloodstream. The release efficiency of DOX under physiological conditions of PBS (pH 7.4 and 5.0) was fully investigated. As depicted in Fig. 3B, DOX@Fe-MOF@PEM released less than 4% of DOX in PBS at pH 7.4, while the nanoparticles released nearly 72% of DOX in PBS at pH 5.0 after 12 h of incubation. Once the pH was lowered, significant sustained release could be observed, and the release efficiency was positively correlated with time, further confirming that PEM-encapsulated nano-ions could effectively control drug release.

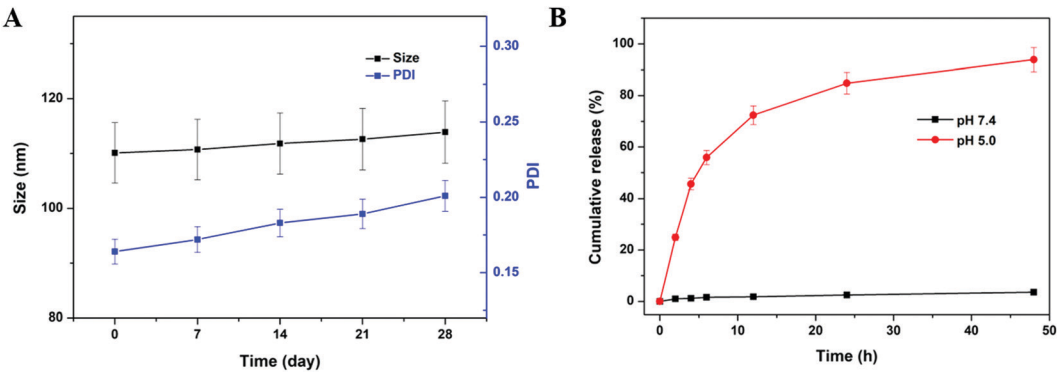

Fig. 3 (A) Changes in the size and PDI of DOX@Fe-MOF@PEM stored at 4 °C in PBS; (B) *in vitro* DOX release profiles of DOX@Fe-MOF@PEM in PBS.

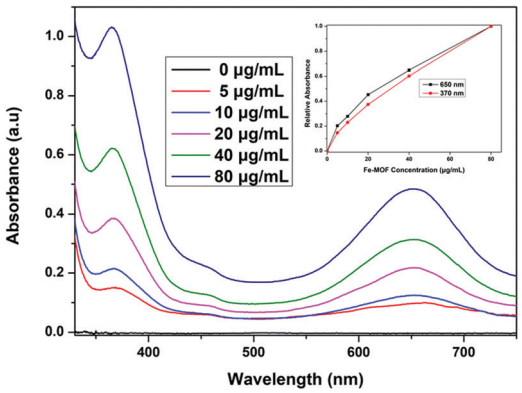

Fig. 4 Absorbance spectra with the addition of Fe-MOF at various concentrations.

3.4. •OH generation

As a typical chromogenic reagent, TMB usually serves as a peroxidase to reduce H_2O_2 to H_2O. Likewise, various concentrations of Fe-MOF have been shown to catalyze the oxidation of TMB by H_2O_2. Research has established that these iron compounds first catalyze H_2O_2 to generate •OH, which oxidizes TMB to form ox-TMB. As shown in Fig. 4, as the concentration of Fe-MOF (0, 5, 10, 20, 40, 80 μg mL^{-1}) increased, the UV absorbance increased. Moreover, the inset shows that the relative absorbance of ox-TMB is a function of Fe-MOF coexistence at 370 and 652 nm.

3.5. Cellular uptake

The internalization of DOX@Fe-MOF and DOX@Fe-MOF@PEM was assessed by CLSM to qualitatively evaluate the cellular uptake of DOX@Fe-MOF@PEM by A549 cells, utilizing the intrinsic red fluorescence of DOX and the blue fluorescent light of DAPI. As could be observed in Fig. 5, after 4 h of incubation, the DOX@Fe-MOF group showed a weak red fluorescence, while the red fluorescence of the DOX@Fe-MOF@PEM group was stronger. The results could be explained by the effective encapsulation of drugs by PEM and thus reduced drug leakage.

3.6. ROS generation

To further evaluate the intracellular ROS generation induced by various formulations, an indicator, 2′,7′-dichlorodihydrofluorescein diacetate (DCFDA), was employed to detect ROS generation, and flow cytometry was applied to explore the changes in the intracellular ROS level of A549 cells. The offset in Fig. 6A could be related to the amount of produced ROS, and a significant difference was noticed in Fig. 6B. The quantity of produced ROS in A549 cells incubated with DOX@Fe-MOF@PEM was 30-fold more than that of the control group and 8.29-fold more than that of DOX. The results indicate that DOX@Fe-MOF@PEM could obviously elevate the intracellular ROS levels.

3.7. *In vitro* cytotoxicity

To assess the antitumor effects of the synthesized nanoparticles, the cytotoxic activity of different formulations was evaluated by MTT assays on A549 and MCF-7 cell lines. As presented in Fig. 7, the Fe-MOF nanoparticles incubated with cancer cells exhibited high cell viability at various concentrations, which firmly verified its relatively low cytotoxicity against cancer cells. As expected, DOX@Fe-MOF at 40 μg mL^{-1} concentration of DOX displayed a stronger inhibitory effect against the cells (83.9% for MCF-7 cells and 83.3% for A549 cells).

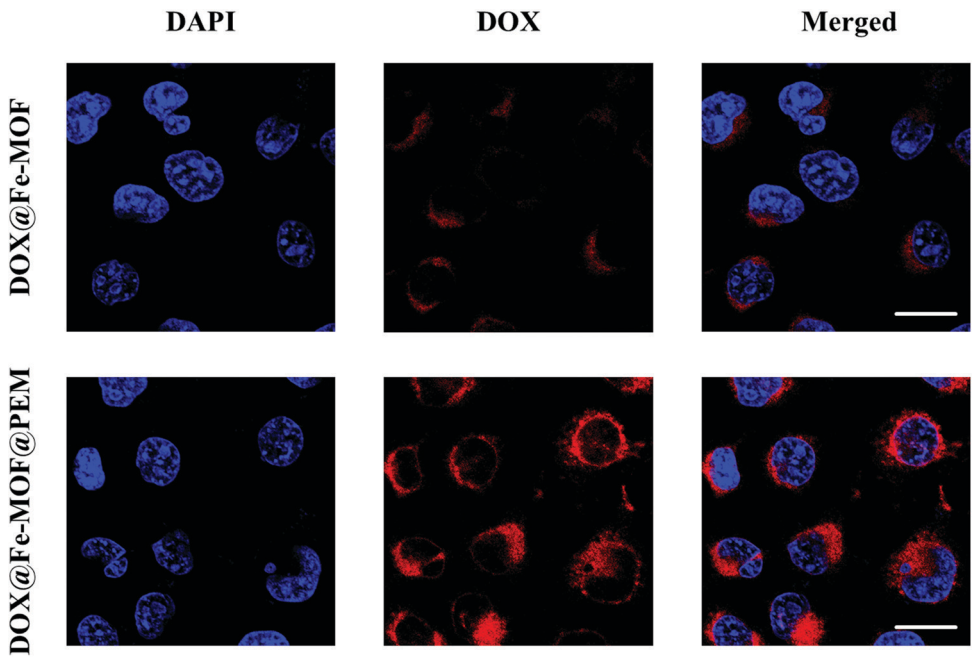

Fig. 5 CLSM images of the A549 cells cultured with DOX@Fe-MOF and DOX@Fe-MOF@PEM. Scale bar: 20 μm.

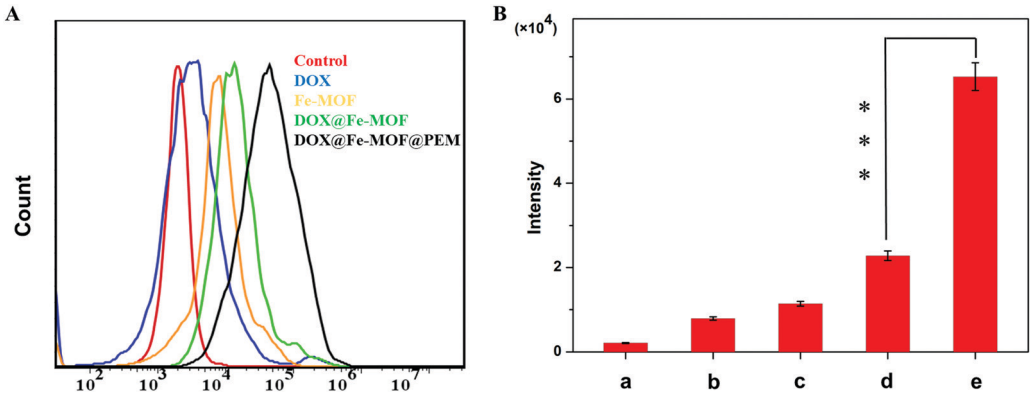

Fig. 6 (A) Quantification ROS intensity of A549 cells induced by different drug formulations, measured by flow cytometry; (B) the analysis of flow cytometry data (a: Control, b: DOX, c: Fe-MOF, d: DOX@Fe-MOF, e: DOX@Fe-MOF@PEM). n = 3, mean ± SD; ***$p < 0.001$.

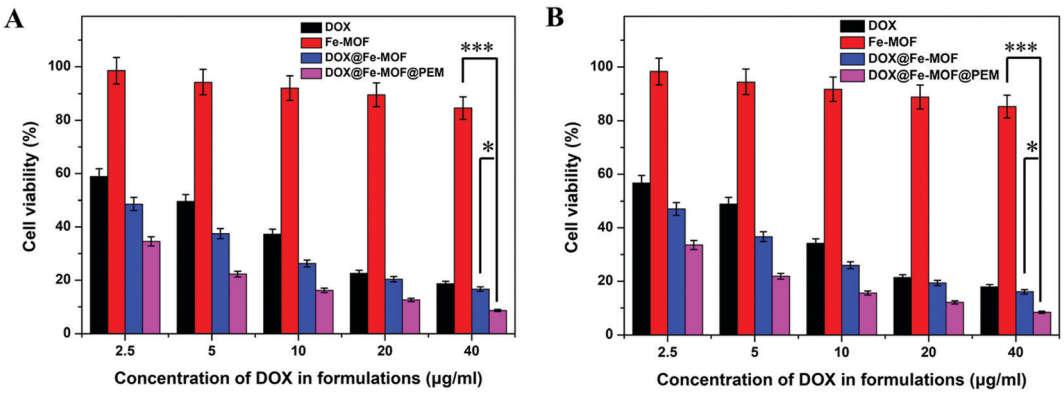

Fig. 7 Relative cell viability of (A) A549 and (B) MCF-7 cells incubated with various formulations. n = 3, mean ± SD; *$p < 0.05$; ***$p < 0.001$.

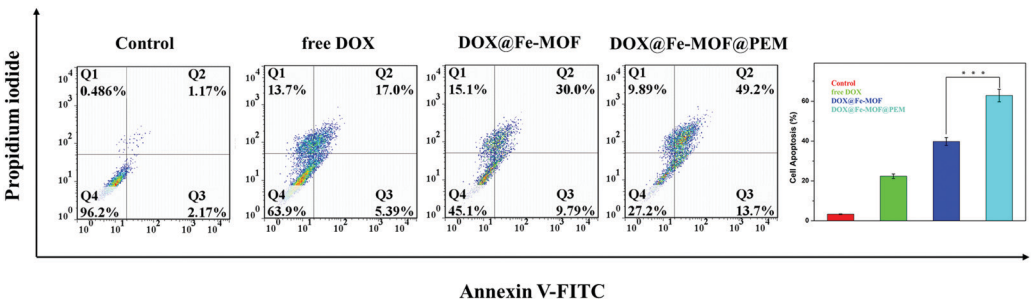

Fig. 8 Apoptosis of A549 cells induced by different formulations achieved using Annexin V-FITC/PI staining. n = 3, mean ± SD; *** $p < 0.001$.

Nevertheless, the cell inhibition ratio of DOX@Fe-MOF@PEM was 91.6% for MCF-7 cells and 91.4% for A549 cells, which was indicative of the role of PEM catalysis in cytotoxicity. In summary, the results revealed that DOX, MOF and PEM possess synergism and heightened cytotoxicity.

3.8. Cell apoptosis

To further explore the effect of nanoparticle-induced apoptosis of A549 cells, the percentage of apoptotic cells in samples treated with Fe-MOF (the control group), free DOX, DOX@Fe-MOF, and DOX@Fe-MOF@PEM at the identical dose of 2.5 μg mL^{-1} DOX for 24 h was determined by flow cytometry. As depicted in Fig. 8, the apoptosis in Fe-MOF displayed a special low rate (3.34%), indicating that Fe-MOF is an extraordinarily safe, biocompatible carrier. Compared with 22.39% of apoptosis induced by free DOX, the cells cultured with DOX@Fe-MOF and DOX@Fe-MOF@PEM exhibited a notable apoptosis ratio of 39.79% and 62.9%, respectively. The outcomes indicate the role of Fe-mediated cell apoptosis and clearly reveal that the prepared DOX@Fe-MOF@PEM could significantly induce apoptosis of A549 cells by the synergy of DOX, MV, and Fe-MOF, which is consistent with the observations from the *in vitro* cytotoxicity test.

4. Conclusions

In summary, a cationic polymer MV-PAH was synthesized rationally, and then a new pH-responsive nanocarrier based on the biocompatible Fe-MOF was effectively built for carrying DOX modified with the cationic polymer MV-PAH multilayers prepared by LBL technique. The PEM decomposed in the weakly acidic environment of tumor cells, significantly enhancing drug delivery. DOX@Fe-MOF@PEM noticeably inhibited the cancer cells in the cytotoxicity and apoptosis experiments. The H_2O_2 induced by DOX and MV-PAH could catalyze the formation of highly toxic ·OH from iron ions in cells through a Fenton-like reaction, simultaneously increasing the anticancer effect of DOX. This original strategy has created a potential way to provide a synergistic effect of ROS and developed a suitable chemotherapy for enhanced anti-cancer efficacy.

Conflicts of interest

There are no conflicts to declare.

Acknowledgements

This work was financially supported by the National Natural Science Foundation of China (Grant No. 21628101 and 21371031), the International S&T Cooperation Program of China (No. 2015DFG42240) and the Priority Academic Program Development (PAPD) of Jiangsu Higher Education Institutions.

References

1 M. L. Circu and T. Y. Aw, *Free Radical Biol. Med.*, 2010, **48**, 749–762.
2 P. T. Schumacker, *Cancer Cell*, 2015, **27**, 156–157.
3 S. Galadari, A. Rahman, S. Pallichankandy and F. Thayyullathil, *Free Radical Biol. Med.*, 2017, **104**, 144–164.
4 J. P. F. Angeli, R. Shah, D. A. Pratt and M. Conrad, *Trends Pharmacol. Sci.*, 2017, **38**, 489–498.
5 S. J. Dixon and B. R. Stockwell, *Nat. Chem. Biol.*, 2014, **10**, 9.
6 H. Wu, F. Chen, D. Gu, C. You and B. Sun, *Nanoscale*, 2020, **12**, 17319–17331.
7 C. Florean, S. Song, M. Dicato and M. Diederich, *Free Radical Biol. Med.*, 2019, **134**, 177–189.
8 J. Kim, J. Kim and J.-S. Bae, *Exp. Mol. Med.*, 2016, **48**, 269.
9 Y. Pan, Z. Luo, X. Wang, Q. Chen, J. Chen, Y. Guan, D. Liu, H. Xua and J. Liu, *Dalton Trans.*, 2020, **49**, 5291–5301.
10 H. Wu, F. Chen, C. You, Y. Zhang, B. Sun and Q. Zhu, *Small*, 2020, **16**, 2001805.
11 K. Sun, Z. Gao, Y. Zhang, H. Wu, C. You, S. Wang, P. An, C. Sun and B. Sun, *J. Mater. Chem. B*, 2018, **6**, 5876–5887.
12 P. a. Ma, H. Xiao, C. Yu, J. Liu, Z. Cheng, H. Song, X. Zhang, C. Li, J. Wang and Z. Gu, *Nano Lett.*, 2017, **17**, 928–937.
13 A. T. Dharmaraja, *J. Med. Chem.*, 2017, **60**, 3221–3240.
14 B. Kwon, E. Han, W. Yang, W. Cho, W. Yoo, J. Hwang, B. M. Kwon and D. Lee, *ACS Appl. Mater. Interfaces*, 2016, **8**, 5887–5897.
15 H. Ranji-Burachaloo, F. Karimi, K. Xie, Q. Fu, P. A. Gurr, D. E. Dunstan and G. G. Qiao, *ACS Appl. Mater. Interfaces*, 2017, **9**, 33599–33608.
16 S. Kwon, H. Ko, D. G. You, K. Kataoka and J. H. Park, *Acc. Chem. Res.*, 2019, **52**, 1771–1782.
17 X. Xu, Z. Dang, T. Sun, S. Zhang and H. Zhang, *Cancer Transl. Med.*, 2018, **4**, 35.
18 Y. Zhong, X. Li, J. Chen, X. Wang, L. Wei, L. Fang, A. Kumar, S. Zhuang and J. Liu, *Dalton Trans*, 2020, **49**, 11045–11058.
19 G. Tan, Y. Zhong, L. Yang, Y. Jiang, J. Liu and F. Ren, *Chem. Eng. J*, 2020, **390**, 124446.
20 R. Oun, Y. E. Moussa and N. J. Wheate, *Dalton Trans*, 2018, **47**, 6645–6653.
21 H. Wu, C. You, F. Chen, J. Jiao, Z. Gao, P. An, B. Sun and R. Chen, *Mater. Sci. Eng., C*, 2019, **103**, 109738.
22 D. Kalyane, N. Raval, R. Maheshwari, V. Tambe, K. Kalia and R. K. Tekade, *Mater. Sci. Eng., C*, 2019, **98**, 1252–1276.
23 T. Sun, Y. S. Zhang, B. Pang, D. C. Hyun, M. Yang and Y. Xia, *Angew. Chem., Int. Ed.*, 2014, **53**, 12320–12364.
24 X. Wang and Z. Guo, *Chem. Soc. Rev.*, 2013, **42**, 202–224.
25 W. Feng, X. Zhou, C. He, K. Qiu, W. Nie, L. Chen, H. Wang, X. Mo and Y. Zhang, *J. Mater. Chem. B*, 2013, **1**, 5886–5898.
26 B.-W. Park, J. Zhuang, O. Yasa and M. Sitti, *ACS Nano*, 2017, **11**, 8910–8923.
27 X. Xie, Y. Zhang, F. Li, T. Lv, Z. Li, H. Chen, L. Jia and Y. Gao, *Curr. Cancer Drug Targets*, 2019, **19**, 257–276.
28 J.-Q. Chu, D.-X. Wang, L.-M. Zhang, M. Cheng, R.-Z. Gao, C.-G. Gu, P.-F. Lang, P.-Q. Liu, L.-N. Zhu and D.-M. Kong, *ACS Appl. Mater. Interfaces*, 2020, **12**, 7575–7585.
29 K. Cheng, Y. Zhang, Y. Li, Z. Gao, F. Chen, K. Sun, P. An, C. Sun, Y. Jiang and B. Sun, *J. Mater. Chem. B*, 2019, **7**, 3291–3302.
30 Z. Shen, T. Liu, Y. Li, J. Lau, Z. Yang, W. Fan, Z. Zhou, C. Shi, C. Ke and V. I. Bregadze, *ACS Nano*, 2018, **12**, 11355–11365.
31 D. Wu, Y. Li, J. Yang, J. Shen, J. Zhou, Q. Hu, G. Yu, G. Tang and X. Chen, *ACS Appl. Mater. Interfaces*, 2017, **9**, 44392–44401.
32 R. Dinis-Oliveira, C. Sousa, F. Remiao, J. Duarte, A. S. Navarro, M. Bastos and F. Carvalho, *Free Radical Biol. Med.*, 2007, **42**, 1017–1028.
33 X. Zhang, Y. Xu, Y. Yang, X. Jin, S. Ye, S. Zhang and L. Jiang, *Chem. – Eur. J*, 2012, **18**, 16411–16418.
34 N. Ma, W.-J. Wang, S. Chen, X.-S. Wang, X.-Q. Wang, S.-B. Wang, J.-Y. Zhu, S.-X. Cheng and X.-Z. Zhang, *Chem. Commun.*, 2015, **51**, 12970–12973.
35 S. Wang, H. Wu, F. Chen, Y. Zhang, Y. Zhang and B. Sun, *RSC Adv.*, 2019, **9**, 33023–33028.
36 C. Stoffelen, J. Voskuhl, P. Jonkheijm and J. Huskens, *Angew. Chem., Int. Ed.*, 2014, **53**, 3400–3404.